

Photoelectric Emission from Dust Grains Exposed to Extreme Ultraviolet and X-ray Radiation

Joseph C. Weingartner¹, B. T. Draine^{2,3}, and David K. Barr¹

ABSTRACT

Photoelectric emission from dust plays an important role in grain charging and gas heating. To date, detailed models of these processes have focused primarily on grains exposed to soft radiation fields. We provide new estimates of the photoelectric yield for neutral and charged carbonaceous and silicate grains, for photon energies exceeding 20 eV. We include the ejection of electrons from both the band structure of the material and the inner shells of the constituent atoms, as well as Auger and secondary electron emission. We apply the model to estimate gas heating rates in planetary nebulae and grain charges in the outflows of broad absorption line quasars. For these applications, secondary emission can be neglected; the combined effect of inner shell and Auger emission is small, though not always negligible. Finally, we investigate the survivability of dust entrained in quasar outflows. The lack of nuclear reddening in broad absorption line quasars may be explained by sputtering of grains in the outflows.

Subject headings: ISM: dust

1. Introduction

Cosmic grains are subjected to electrical charging processes and the resulting non-zero charge can have important astrophysical consequences. In Galactic H I regions, the grain charge is primarily determined by a balance between starlight-induced photoelectric emission and the collisional capture of electrons from the gas. Furthermore, in these regions the gas heating is dominated by photoelectric emission from dust. Thus, there have been numerous detailed studies of UV-induced photoelectric emission (Spitzer 1948; Watson 1972; de Jong

¹Department of Physics and Astronomy, George Mason University, MSN 3F3, 4400 University Drive, Fairfax, VA 22030, USA; joe@physics.gmu.edu, dbarr@physics.gmu.edu

²Princeton University Observatory, Peyton Hall, Princeton, NJ 08544, USA; draine@astro.princeton.edu

³Osservatorio Astrofisico di Arcetri, Largo E Fermi 5, 50125 Firenze, Italy

1977; Draine 1978; Tielens & Hollenbach 1985; Bakes & Tielens 1994; Weingartner & Draine 2001b).

Photoelectric emission from grains exposed to extreme ultraviolet (EUV) and X-ray radiation has received much less attention. Dwek & Smith (1996) modelled, in detail, the dust and gas heating for neutral grains exposed to high-energy radiation, but did not address the grain charging.

Charging by high-energy photons can be very important for grains immersed in hot plasma and exposed to a hard radiation field. The grain potential is limited by the highest photon energy present in the incident radiation; as this increases, the grain can reach higher potentials. The efficiency of the gas heating decreases as the grain charge increases, since the photoelectrons have to climb out of the potential well.

Hard radiation fields can be found, e.g., in planetary nebulae and active galactic nuclei (AGNs). If the gas contains dust, then a fraction of the incident radiation will be processed into infrared (IR) radiation, i.e., thermal dust emission. Dwek & Smith (1996) were motivated by the prospect of learning about these environments through the analysis of the IR emission. Ferland et al. (2002) stressed that the X-ray and IR spectra in AGNs may be correlated as a result of the interaction between hot grains and gas. Detailed modelling of these regions will only be possible once the grain charging is properly modelled, since the grain and gas heating rates depend on the charging.

In a previous paper (Weingartner & Draine 2001b, hereafter WD01), we modelled in detail the photoelectric emission from grains exposed to UV radiation; this is briefly summarized in §2. In §§3 through 8, we extend the WD01 model to include EUV and X-ray radiation. Applications to planetary nebulae and quasar outflows are described in §9 and §10, respectively.

2. Photoelectric Emission Induced by Low-Energy Photons

As a starting point for this study, we will adopt the WD01 photoelectric emission model. Here, we briefly discuss some of the important features of this model and mention two minor modifications.

The photoelectric emission rate depends on the absorption cross section and the photoelectric yield Y (i.e., the probability that an electron will be emitted following the absorption of a photon), both of which depend on the photon energy $h\nu$.

WD01 assumed spherical grains, for which the absorption cross section is $Q_{\text{abs}}\pi a^2$, where

a is the grain radius and Q_{abs} is the absorption efficiency factor. They used Mie theory to compute Q_{abs} and adopted dielectric functions from Li & Draine (2001) and Weingartner & Draine (2001). Here, we will use Mie theory to compute Q_{abs} when $x \equiv 2\pi a/\lambda < 2 \times 10^4$ (λ is the wavelength of the radiation) and anomalous diffraction theory when $x > 2 \times 10^4$ (Draine 2003). We also will use somewhat newer dielectric functions (Draine 2003).

The WD01 prescription for determining the threshold photon energy for photoelectric emission, $h\nu_{\text{pet}}$, is discussed in their §§2.2 and 2.3.1 and equations 2 through 7. Here, we will adopt a different expression for the minimum energy that an electron must have to escape a negatively-charged grain, E_{min} . Instead of equation 7 from WD01, we adopt equation 1 from van Hoof et al. (2004).¹ Thus, $h\nu_{\text{pet}}$ for photoelectric emission from the band structure is taken to be

$$h\nu_{\text{pet}}(Z, a) = \begin{cases} \text{IP}_V(Z, a) & , Z \geq -1 \\ \text{IP}_V(Z, a) + E_{\text{min}}(Z, a) & , Z < -1 \end{cases} \quad (1)$$

with the “valence band ionization potential”

$$\text{IP}_V(Z, a) = W + \left(Z + \frac{1}{2}\right) \frac{e^2}{a} + (Z + 2) \frac{e^2 0.3 \text{ \AA}}{a} \quad (2)$$

and

$$E_{\text{min}} = \begin{cases} 0 & , Z \geq -1 \\ \theta_\nu(\nu = |Z + 1|) [1 - 0.3(a/10 \text{ \AA})^{-0.45}|Z + 1|^{-0.26}] & , Z < -1 \end{cases} ; \quad (3)$$

W is the work function and θ_ν is defined in equation 2.4 of Draine & Sutin (1987). We retain the WD01 estimates of $W = 4.4 \text{ eV}$ (8 eV) for carbonaceous (silicate) grains.

WD01 adopted the following expression for the photoelectric yield of a grain with charge Ze (their equation 12; e is the proton charge):

$$Y(h\nu, Z, a) = y_2(h\nu, Z, a) \times \min [y_0(\Theta)y_1(a, h\nu), 1] \quad , \quad (4)$$

where

$$\Theta = \begin{cases} h\nu - h\nu_{\text{pet}} + (Z + 1)e^2/a & , Z \geq 0 \\ h\nu - h\nu_{\text{pet}} & , Z < 0 \end{cases} \quad (5)$$

(WD01 equation 9). For a bulk solid, $Y(h\nu) = y_0(\Theta = h\nu - W)$. WD01 present approximations, derived from laboratory measurements, for $y_0(\Theta)$ for carbonaceous and silicate grains (their equations 16 and 17, respectively).

¹Since van Hoof et al. (2004) define E_{min} as the negative of our E_{min} , the minus sign in their equation 1 is absent here.

We adopt the size-dependent yield enhancement factor y_1 used by WD01:

$$y_1(a, h\nu) = \left(\frac{\beta}{\alpha}\right)^2 \frac{\alpha^2 - 2\alpha + 2 - 2\exp(-\alpha)}{\beta^2 - 2\beta + 2 - 2\exp(-\beta)} \quad (6)$$

where $\beta \equiv a/l_a$ and $\alpha \equiv a/l_a + a/l_e$. It depends on the photon attenuation length, l_a (the e -folding length for the decrease of radiation intensity as it propagates into the material) and the electron escape length, l_e (roughly the distance that the electron travels in the material before losing its energy). The electron escape length depends on the energy of the excited photoelectron; WD01 adopted $l_e = 10 \text{ \AA}$ in all cases, which is a reasonable approximation for the low-energy electrons excited by visible and UV radiation.

Finally, the factor $y_2(h\nu, Z, a)$ accounts for the fact that not all of the electrons that breach the surface barrier have sufficient energy to escape to infinity. WD01 assumed a parabolic electron energy distribution:

$$f_E^0(E) = \frac{6(E - E_{\text{low}})(E_{\text{high}} - E)}{(E_{\text{high}} - E_{\text{low}})^3} \quad , \quad E_{\text{low}} \leq E \leq E_{\text{high}} \quad , \quad (7)$$

where $f_E^0(E)dE$ gives the fraction of attempting electrons with energy (with respect to infinity) between E and $E + dE$. When $Z < 0$, $E_{\text{low}} = E_{\text{min}}$ and $E_{\text{high}} = E_{\text{min}} + h\nu - h\nu_{\text{pet}}$; when $Z \geq 0$, $E_{\text{low}} = -(Z + 1)e^2/a$ and $E_{\text{high}} = h\nu - h\nu_{\text{pet}}$. The fraction of attempting electrons that escape to infinity is given by

$$y_2(h\nu, Z, a) = \begin{cases} \int_0^{E_{\text{high}}} dE f_E^0(E) = E_{\text{high}}^2 (E_{\text{high}} - 3E_{\text{low}})/(E_{\text{high}} - E_{\text{low}})^3 & , Z \geq 0 \\ 1 & , Z < 0 \end{cases} \quad . \quad (8)$$

3. Photoelectric Emission Induced by High-Energy Photons

Photoelectric emission induced by high-energy photons differs from that induced by low-energy photons in the following ways:

1. Whereas low-energy photons can only excite electrons from the band structure of the solid, high-energy photons can also excite inner shell electrons. Except very near the absorption edge (see, e.g., Draine 2003) the absorption cross section from inner shell electrons will be essentially identical to that for isolated atoms. Dwek & Smith (1996) find that the transition between band-like and atomic-like absorption typically occurs for photon energies around 50 eV. However, laboratory-measured photoelectron yields are only available for $h\nu$ up to $\approx 20 \text{ eV}$.

2. A sufficiently energetic photon can excite a photoelectron from atomic shells other than the highest occupied shell (e.g., from the 1s shell in C if $h\nu > 291 \text{ eV}$). The hole left by

the photoelectron can then be filled in a radiationless transition in which a second electron fills the vacancy produced by the photoionization, with the excess binding energy going into kinetic energy of a third electron, which then leaves the atom (the Auger effect). The Auger electron can then possibly leave the grain. This process can give rise to a cascade of secondary Auger transitions that fill holes produced in previous Auger transitions. Thus, more than one electron can be emitted from a grain following the absorption of a high-energy photon.

3. Following the absorption of a high-energy photon, the photoelectrons and Auger electrons might have enough energy to excite secondary electrons from the grain.

In the following sections, we will discuss the emission of primary photoelectrons, Auger electrons, and secondary electrons.

4. Emission of Primary Photoelectrons

4.1. Bulk Yields

4.1.1. Physical Model

In the case of high-energy radiation, we assume atomic-like absorption and estimate the bulk yield of photoelectrons ejected from each shell of each atomic constituent of the grain: $y_0(i, s; \Theta_{i,s})$ is the probability that a primary photoelectron excited from shell s of element i escapes the bulk solid following the absorption of a photon of energy $h\nu = \Theta_{i,s} + I_{i,s}$, where $I_{i,s}$ is the ionization energy of shell s of element i .

To estimate the bulk photoelectron yields, we adopt a semi-infinite slab geometry and assume that a photoelectron escapes the solid with probability $0.5 \exp(-z/l_e)$, where z is the perpendicular distance between the surface and the point of excitation. The factor 0.5 accounts for the fact that only half of the photoelectrons will travel towards the surface of the solid, if they are emitted isotropically. For simplicity, we ignore refraction and the fact that the reflectivity varies with the angle of incidence, θ . For an isotropic incident radiation field,

$$y_0(i, s; \Theta_{i,s}) = n_i \sigma_{i,s} l_a \int_0^{\pi/2} d\theta \sin \theta \cos \theta \int_0^\infty \frac{dx}{l_a} \exp \left[-x \left(\frac{1}{l_a} + \frac{\cos \theta}{l_e} \right) \right] = n_i \sigma_{i,s} l_e \left[1 - \frac{l_e}{l_a} \ln \left(1 + \frac{l_a}{l_e} \right) \right] ; \quad (9)$$

x is the distance along an incident ray from the surface and $n_i \sigma_{i,s} l_a$ is the probability that absorption is by shell s of element i . In evaluating $\sigma_{i,s} l_a$, the photon energy $h\nu = \Theta_{i,s} + I_{i,s}$; in evaluating l_e , the initial energy of the excited photoelectron $E_e = h\nu - I_{i,s} = \Theta_{i,s}$. To find

the bulk yield of photoelectrons ejected from the band structure, $y_0(\text{band}, \Theta_{\text{band}})$, we sum $y_0(i, s)$ over all of the shells that comprise the band, except that we take $E_e = \Theta_{\text{band}}$ and $h\nu = \Theta_{\text{band}} + W$. We take photoionization cross sections from Verner & Yakovlev (1995) and Verner et al. (1996), making use of the FORTRAN routine *phfit2*.²

The photon absorption length $l_a = \lambda/(4\pi \text{Im } m)$, where λ is the wavelength *in vacuo* and $m(\lambda)$ is the complex refractive index, can be approximated by

$$l_a^{-1}(h\nu) = \sum_{i,s} n_i \sigma_{i,s}(h\nu) \quad . \quad (10)$$

For consistency with our atomistic approach to photoelectric emission, we will use the approximation when $h\nu > 20 \text{ eV}$.

4.1.2. Electron Escape Length

WD01 took $l_e = 10 \text{ \AA}$ for $h\nu \lesssim 20 \text{ eV}$, in approximate agreement with experiments on C (Martin et al. 1987) and SiO_2 (McFeely et al. 1990) films. For high initial energies E_e , the electron escape length is roughly given by (Draine & Salpeter 1979)

$$l_e(E_e) \approx 300 \text{ \AA} \left(\frac{\rho}{\text{g cm}^{-3}} \right)^{-0.85} \left(\frac{E_e}{\text{keV}} \right)^{1.5} \quad , \quad 300 \text{ eV} < E_e < 1 \text{ MeV} \quad , \quad (11)$$

where ρ is the density of the material. Extending equation (11) below 300 eV, we would find $l_e = 10 \text{ \AA}$ at $E_e = 164 \text{ eV}$ for carbonaceous grains (assuming the ideal graphite density of $\rho = 2.24 \text{ g cm}^{-3}$) and at $E_e = 211 \text{ eV}$ for silicates (assuming $\rho = 3.5 \text{ g cm}^{-3}$). The upturn in l_e at $\sim 200 \text{ eV}$ for C is in rough agreement with the results of Martin et al. (1987), who considered E_e up to 1 keV. Thus, we adopt

$$l_e(E_e; \text{carbonaceous}) = \begin{cases} 10 \text{ \AA} & , E_e \leq 164 \text{ eV} \\ 4.78 \times 10^{-3} \text{ \AA} (E_e/\text{eV})^{1.5} & , E_e > 164 \text{ eV} \end{cases} \quad (12)$$

and

$$l_e(E_e; \text{silicate}) = \begin{cases} 10 \text{ \AA} & , E_e \leq 211 \text{ eV} \\ 3.27 \times 10^{-3} \text{ \AA} (E_e/\text{eV})^{1.5} & , E_e > 211 \text{ eV} \end{cases} \quad . \quad (13)$$

²The subroutine *phfit2* was written by D. A. Verner and is available at <http://www.pa.uky.edu/~verner/fortran.html>.

4.1.3. Carbonaceous Grains

We adopt the ideal graphite density of 2.24 g cm^{-3} ; thus, the C atom number density $n_{\text{C}} = 1.12 \times 10^{23} \text{ cm}^{-3}$. There are strong correlations between the 2s and 2p shells, with no jump in the photoionization cross section at the 2s threshold (Verner et al. 1996). Thus, we treat (2s + 2p) as a single shell, with ionization energy equal to that of the 2p shell = 11.26 eV. (See Table 1 for the ionization energies of relevant elements.) The bulk yield computed using equation (9) is displayed as the short-dashed curve in Figure 1. Since the (2s + 2p) shell produces the band structure, this high-energy yield curve should connect continuously with the low-energy curve from WD01 (their equation 16), which is displayed as the long-dashed curve in Figure 1. To enforce this continuity, we adopt the yield computed here when $h\nu > 50 \text{ eV}$, the WD01 yield when $h\nu < 20 \text{ eV}$, and interpolate between these when $20 \text{ eV} < h\nu < 50 \text{ eV}$. The result is displayed as the solid curve in Figure 1.

4.1.4. Silicate Grains

For silicate grains, we adopt a stoichiometry approximating MgFeSiO_4 and a density of 3.5 g cm^{-3} , intermediate between the values for crystalline forsterite (Mg_2SiO_4 , 3.21 g cm^{-3}) and fayalite (Fe_2SiO_4 , 4.39 g cm^{-3}). The atomic number densities are thus $n_{\text{Mg}} = n_{\text{Fe}} = n_{\text{Si}} = 1.22 \times 10^{22} \text{ cm}^{-3}$ and $n_{\text{O}} = 4.88 \times 10^{22} \text{ cm}^{-3}$.

As with C (2s + 2p), O (2s + 2p), Si (3s + 3p), and Fe (3d + 4s) do not display jumps in the photoionization cross section at the threshold energy of the deeper shell. Thus, we treat each of these pairs as a single shell, with ionization energy equal to that of the lower-energy shell. The O 2s and 2p, Si 3s and 3p, Mg 3s, and Fe 3d and 4s shells are considered to comprise the silicate band structure. As with graphite, we adopt the WD01 yield when $h\nu < 20 \text{ eV}$, the yield computed here when $h\nu > 50 \text{ eV}$, and interpolate between these when $20 \text{ eV} < h\nu < 50 \text{ eV}$. The resulting yield is displayed in Figure 2.

4.2. Size-Dependent Yield

For photoelectric emission from the band structure of carbonaceous and silicate grains, we compute $y_1(h\nu, a)$ and $y_2(h\nu, Z, a)$ using the WD01 prescription, as modified in §2 above (eqs. 6 and 8). We estimate $y_0(\Theta_{\text{band}})$ as discussed in §§4.1.3 and 4.1.4; Θ_{band} is computed using equation (5). Equation (4) is employed to compute the yield, except that the 1 in the min function is replaced by the probability P_{band} that the photon absorption occurs in the

band structure, rather than in an inner shell. We estimate

$$P_{\text{band}}(h\nu) \approx l_a(h\nu) \sum_{i,s}^{\text{band}} n_i \sigma_{i,s}(h\nu) \quad , \quad (14)$$

where the sum is over all shells that are taken to comprise the band structure (see §§4.1.3 and 4.1.4).

The yield for photoelectric emission from the inner shells is computed in exactly the same way, except that the work function is replaced by the appropriate ionization energy when computing the photoelectric threshold energy, $h\nu_{\text{pet}}$ (which is needed to evaluate $\Theta_{i,s}$; see eq. 5). Also, P_{band} is replaced with $P_{i,s} = l_a n_i \sigma_{i,s}$.

Very small carbonaceous grains are taken to be polycyclic aromatic hydrocarbons (PAHs). For these, we expect $Y \rightarrow 1$ as $h\nu \rightarrow \infty$ for the electrons associated with the “band structure”. This applies by construction for the WD01 yields, but does not apply to the yields derived here. Thus, when $a \leq 6 \text{ \AA}$ (corresponding to ≈ 100 C atoms; see eq. 1 in WD01), we employ y_0 from WD01. When $6 \text{ \AA} < a \leq 13 \text{ \AA}$, we take

$$y_{0,\text{band}} = y_{0,\text{band}}(\text{WD01}) \frac{13 \text{ \AA} - a}{7 \text{ \AA}} + y_{0,\text{band}}(\text{this work}) \frac{a - 6 \text{ \AA}}{7 \text{ \AA}} \quad . \quad (15)$$

5. Emission of Auger Electrons

Suppose a primary photoelectron is ejected from shell s of element i . There are a number of Auger transitions that can then occur; we will denote them with index j . Adopting the model for electron escape from §4.1.1, the bulk yield for the j -th Auger transition is

$$y_{0,A}(i, s, j; \Theta_{A;i,s}) = p_{A,i,s,j} n_i \sigma_{i,s} l_e \left[1 - \frac{l_e}{l_a} \ln \left(1 + \frac{l_a}{l_e} \right) \right] \quad , \quad (16)$$

where $p_{A,i,s,j}$ is the average number of electrons ejected from the atom via Auger transition j , photon energy $h\nu = \Theta_{A;i,s} + I_{i,s}$ is used in evaluating $\sigma_{i,s}$ and l_a , and the energy $E_{A,i,s,j}$ of the Auger electron is used when evaluating l_e . We adopt the values of $p_{A,i,s,j}$ and $E_{A,i,s,j}$ given in Tables 4.1 and 4.2 of Dwek & Smith (1996). Note that the Auger yield is the average number of electrons emitted by the grain via the given Auger transition, rather than the probability of electron emission, and may exceed unity.

For all grain sizes and charges, we take the threshold photon energy equal to $I_{i,s}$, even though it should really be somewhat less than this, due to the presence of the band structure. We use equation (4) to evaluate the Auger electron yield $Y_{A,j}$, except that the 1 in the min

function is replaced with $Y_{A,i,s,j;\max} = P_{i,s} p_{A,i,s,j}$. We also adopt somewhat different values of the input energies than for the case of primary photoelectrons. In evaluating $y_{0,A}$, we take $\Theta_{A;i,s} = h\nu - I_{i,s}$, regardless of grain size and charge. In computing $y_1(h\nu, a)$, we take $E_e = E_{A,i,s,j}$ (when evaluating l_e). We use equation (8) to compute $y_2(h\nu, Z, a)$ with $E_{\text{high}} = E_{A,i,s,j} - (Z + 1)e^2/a$; $E_{\text{low}} = E_{\text{min}}$ when $Z < 0$ and $E_{\text{low}} = -(Z + 1)e^2/a$ when $Z \geq 0$. For Auger electrons, it can occur that $E_{\text{high}} < 0$; in this case, we set $y_2 = 0$.

6. Emission of Secondary Electrons

The secondary electron yield is defined as the average number of secondary electrons emitted per absorbed photon; it may exceed unity. This yield can be expressed as a sum of partial yields (denoted with index k), with a term for each type of process that can excite a secondary electron (namely, primary emission from the band structure and inner shells and Auger emission):

$$Y_{\text{sec}}(h\nu, Z, a) = \sum_k Y_{\text{sec},k}(h\nu, Z, a) \quad . \quad (17)$$

Since secondary electron energies are generally low, only those excited close to the surface have significant probability of escape. Thus, we take $Y_{\text{sec},k} = 0$ if $Y_k = 0$; otherwise, we approximate

$$Y_{\text{sec},k}(h\nu, Z, a) = Y_k(h\nu, Z, a) \frac{y_{2,k}^{\text{sec}}(h\nu, Z, a) E_{e,k}}{y_{2,k}(h\nu, Z, a) \epsilon} \frac{l_e^{-1}(E_{e,k})}{a^{-1} + (10 \text{ \AA})^{-1}} \quad (18)$$

where $E_{e,k} = h\nu - W$ for primary electrons excited from the band structure, $h\nu - I_{i,s}$ for primary electrons excited from inner shell (i, s), and $E_{A,i,s,j}$ for an Auger electron; ϵ is the average energy loss by the exciting electron per secondary electron created in the solid. Draine & Salpeter (1979) estimate that $\epsilon = 117 \text{ eV}$ for graphite and 155 eV for lunar dust; we will adopt these values for carbonaceous and silicate grains. The grain size a is included in the last factor to account for the fact that the exciting electron may escape the grain before producing secondary electrons.

For the secondary electron energy distribution, we adopt

$$f_E^0(E) = \frac{\alpha \tilde{E}^{-2}(E - E_{\text{low}})}{\left[1 + \tilde{E}^{-2}(E - E_{\text{low}})^2\right]^{3/2}} \quad (19)$$

(Draine & Salpeter 1979) with $\tilde{E}^2 = 8 \text{ eV}^2$ and normalization factor

$$\alpha = \left\{ 1 - \left[1 + \tilde{E}^{-2}(E_{\text{high}} - E_{\text{low}})^2 \right]^{-1/2} \right\}^{-1} \quad . \quad (20)$$

Thus,

$$y_{2,k}^{\text{sec}}(h\nu, Z, a) = \begin{cases} \alpha \left\{ \left[1 + \tilde{E}^{-2} E_{\text{low}}^2 \right]^{-1/2} - \left[1 + \tilde{E}^{-2} (E_{\text{high}} - E_{\text{low}})^2 \right]^{-1/2} \right\} & , Z \geq 0 \\ 1 & , Z < 0 \end{cases} \quad (21)$$

when $E_{\text{high}} > 0$; otherwise, $y_{2,k}^{\text{sec}} = 0$. For secondary electrons excited by a primary photoelectron, we take E_{low} and E_{high} to be the same as for the primary; likewise for those excited by Auger electrons. Consequently, the threshold photon energies for the emission of secondary electrons are equal to those for the electrons that excite them.

Figure 3 displays the yields of primary, Auger, and secondary electrons for carbonaceous grains with $a = 0.1\mu\text{m}$. The primary yield Y_p reaches unity at $h\nu = 10^4\text{eV}$, where both l_a and l_e are very large. However, $Q_{\text{abs}}Y_p$ is a decreasing function at high photon energy. Figures 4 and 5 display the total yield (primary plus Auger plus secondary) for carbonaceous and silicate grains of various sizes.

7. Total Photoelectric Emission Rate and Grain Charging

The primary photoelectric emission rate (excluding that due to excess “attached” electrons on negatively charged grains) is

$$J_{\text{pe}} = \pi a^2 \int_{\nu_{\text{pet}}(\text{band})}^{\nu_{\text{max}}} d\nu \frac{cu_\nu}{h\nu} Q_{\text{abs}} \left(Y_{p;\text{band}} + \sum_{i,s} Y_{p;i,s} \right) \quad (22)$$

(c.f. eq. 25 in WD01); $h\nu_{\text{max}}$ is the highest photon energy in the incident radiation field and Y_p denotes the yield of primary electrons. For negatively charged grains, the excess electrons undergo photodetachment at a rate

$$J_{\text{pd}} = \int_{\nu_{\text{pdt}}}^{\nu_{\text{max}}} d\nu \frac{cu_\nu}{h\nu} \sigma_{\text{pdt}} \quad ; \quad (23)$$

the photodetachment threshold energy and cross section are taken from equations 18 and 19 in WD01, respectively. The Auger electron emission rate is

$$J_A = \pi a^2 \int_{I_{is,\text{min}}/h}^{\nu_{\text{max}}} d\nu \frac{cu_\nu}{h\nu} Q_{\text{abs}} \sum_{i,s,j} Y_{A;i,s,j} \quad , \quad (24)$$

where $I_{is,\text{min}}$ is the lowest ionization energy among those of the inner shells. Of course, for all shells the yields are zero when $h\nu < h\nu_{\text{pet}}$. The emission rate of secondary electrons (excited

by primary photoelectrons and Auger electrons) is

$$J_{\text{sec, pe}} = \pi a^2 \int_{\nu_{\text{pet}}(\text{band})}^{\nu_{\text{max}}} d\nu \frac{cu_\nu}{h\nu} Q_{\text{abs}} \sum_k Y_{\text{sec, } k} \quad , \quad (25)$$

where the sum over k denotes the sum over all exciting primary and Auger electrons.

The collisional charging rates due to positive ions (assumed to have charge e) and electrons are denoted J_{ion} and J_e , respectively, and are computed as described in §§2.4 and 3 in WD01. Since we will be considering high-temperature gas here, we also include secondary emission induced by incident gas-phase electrons. We compute the charging rate $J_{\text{sec, gas}}$ using the Draine & Salpeter (1979) model (their eqs. 14 through 16 and A7 through A11).

When each charging event involves the transfer of a single charge quantum $\pm e$, statistical equilibrium yields

$$f_Z(Z)[J_{\text{pe}}(Z) + J_A(Z) + J_{\text{sec, pe}}(Z) + J_{\text{pd}}(Z) + J_{\text{ion}}(Z) + J_{\text{sec, gas}}] = f_Z(Z+1)J_e(Z+1) \quad , \quad (26)$$

where $f_Z(Z)$ is the probability for the grain charge to be Ze . WD01 used this equation (without J_A , $J_{\text{sec, pe}}$, and $J_{\text{sec, gas}}$) to solve for the grain charge distribution. When Auger and secondary emission are important, more than one electron can be emitted at a time, yielding a slightly more complicated balance equation and a very complicated combinatorics problem. To simplify matters, we will continue to use equation (26). We also compute a single “equilibrium charge”, i.e., the charge for which the net current $J_{\text{pe}} + J_{\text{pd}} + J_A + J_{\text{sec, pe}} + J_{\text{ion}} + J_{\text{sec, gas}} - J_e$ equals zero. For large grains, the equilibrium charge is nearly identical to the average over the charge distribution. Even for small grains, the difference is not large when the grain is highly charged. In the following sections, we will present results obtained by resolving the charge distribution, unless otherwise indicated.

A rigorous treatment of multi-electron ejection events would increase the value of Z when computing potentials and yields for successive escaping electrons. We will ignore this complication as well.

8. Gas Heating

The photoelectric gas heating rate per grain with charge Ze , due to primary photoelectrons originating in the band structure, is given by

$$\Gamma'_{\text{pe}}(a) = \pi a^2 \int_{\nu_{\text{pet}}(\text{band})}^{\nu_{\text{max}}} d\nu \frac{cu_\nu}{h\nu} Q_{\text{abs}} Y_{p;\text{band}} \int_{E_{\text{min}}(\text{band})}^{E_{\text{max}}(\text{band})} dE f_E(\text{band}; E) E \quad , \quad (27)$$

where E_{\min} is given by equation (3), $E_{\max} = h\nu - h\nu_{\text{pet}} + E_{\min}$, and $f_E(E) = f_E^0(E)/y_2$. The heating rate due to primary electrons originating in inner shell (i, s) , $\Gamma'_{\text{pe};i,s}$, is identical, except that each quantity in equation (27) is evaluated for (i, s) . Similarly for the heating rate due to Auger and secondary electrons, except that $E_{\max} = I_{i,s} - (Z + 1)e^2/a$ for Auger emission and secondary emission excited by Auger electrons; $I_{i,s}$ is the ionization energy of the shell in which the primary excitation occurs. The heating rate due to photodetachment is given in eq. 40 of WD01.

The gas cooling rate per grain due to recombination of charged particles with the grain, Λ'_{gr} , is computed as described in §5 of WD01. The cooling is reduced when secondary electrons are ejected. We make a simple estimate of this reduction by assuming that the average energy (with respect to infinity) of escaping secondary electrons is

$$\bar{E} = \frac{\int_{E_1}^{\langle E_0 \rangle} dE f_E^0(E)(E - e\phi)}{\int_{E_1}^{\langle E_0 \rangle} dE f_E^0(E)} \quad (28)$$

where $\langle E_0 \rangle$ is the average energy of the incident electrons (eq. 16 in Draine & Salpeter 1979), ϕ is the grain potential, f_E^0 is given by equation (19) with $E_{\text{low}} = 0$ and $E_{\text{high}} = \langle E_0 \rangle$, and $E_1 = 0$ when $Z < 0$ and $e\phi$ when $Z \geq 0$.

9. Planetary Nebulae

A planetary nebula is exposed to a hard radiation field from the hot central star, and photoelectric emission from dust is an important mechanism for heating the gas (Dopita & Sutherland 2000; van Hoof et al. 2004).

In Table 2, we display photoelectric heating rates Γ_{pe} and collisional cooling rates Λ for a model planetary nebula and several different grain size distributions. We assume that the radiation field is a blackbody with a color temperature $T_c = 2 \times 10^5$ K and intensity $G = 2 \times 10^3$. ($G \equiv u_{\text{rad}}^{\text{uv}}/u_{\text{Hab}}^{\text{uv}}$, where $u_{\text{rad}}^{\text{uv}}$ is the energy density in the radiation field between 6 eV and 13.6 eV and $u_{\text{Hab}}^{\text{uv}} = 5.33 \times 10^{-14}$ erg cm $^{-3}$ is the Habing (1968) estimate of the starlight energy density in this range.) This intensity corresponds to a distance of 10^{17} cm from a star with luminosity $10^4 L_{\odot}$. We adopt a fully ionized H nebula with number density $n_{\text{H}} = 10^3$ cm $^{-3}$ and temperature $T = 10^4$ K.

The dust in a planetary nebula is unlikely to be the same as the average interstellar dust modeled by Weingartner & Draine (2001a). We assume that either carbonaceous grains or silicate grains are present, but not both. The size distributions for either the carbonaceous grains or the silicate grains are taken from the size distribution for the appropriate compo-

ment in various dust models developed by Weingartner & Draine (2001a). These reproduce extinction laws with $R_V = A_V/E(B - V) = 3.1, 4, \text{ or } 5.5$, for various values of the amount b_C of carbon per interstellar H atom in PAHs, with cases “A” and “B” referring to different assumptions made concerning the total amount of material in the interstellar grain model. The photoelectric heating contribution $\Gamma_{\text{pe}}/(Gn_{\text{H}})$ of the silicate component varies from 3.6 to $23 \times 10^{-25} \text{ ergs}^{-1}$ – more than a factor 6 – showing the sensitivity to the actual size distribution. The heating and cooling rates in Table 2 should be taken as an indication of the general magnitude that Γ_{pe} and Λ can have.

For carbonaceous dust, use of the WD01 yields overestimates the heating rate by a factor of 1.1 to 2 and the cooling rate by as much as 28% (for the first entry in Table 2). Inner shell and Auger emission are unimportant, and secondary emission contributes only at the 5% level or less. For silicate dust, the heating (cooling) rate is overestimated by a factor of ≈ 1.9 to 2.5 (1.3 to 1.5) when the WD01 yields are employed. Inner shell and Auger emission account for about 10% of the total heating and secondary emission contributes at the 5 to 10% level. For both types of dust, the heating (cooling) results differ by at most 5% (1%) when secondary emission induced by incident gas-phase electrons is ignored.

Since the adopted photoelectric yields are highly uncertain, we also computed the heating and cooling rates with the bulk yields increased and decreased by a factor 2. For carbonaceous grains, the maximal changes in the heating (cooling) rates were $\approx 30\%$ (20%). For silicate grains, the revised yields resulted in changes of factors ≈ 1.5 and 0.6 for the heating rate; the cooling rate was somewhat less sensitive to the changes in the yield.

10. Quasar Outflows

X-ray observations of broad absorption line quasars (BALQSOs) reveal large columns of absorbing material (e.g., Gallagher et al. 2002). Optical observations, on the other hand, indicate that the nucleus is not substantially reddened (e.g., Reichard et al. 2003). Thus, it appears that the outflows either are dust-free or contain only very large (by interstellar standards) grains. One possible explanation is that the dust is destroyed by sputtering in the hot gas. In this process, energetic gas-phase ions collide with the grain and eject surface atoms into the gas. There are two limiting regimes for sputtering: “thermal” sputtering, where the drift velocity of the grain is negligible compared to the thermal motions of the ions, and “drift” sputtering, where the relative velocity of impinging ions is due primarily to motion of the grain through the gas. In the presence of a hard radiation field, the grains may acquire large, positive electric potentials, suppressing destruction by sputtering (Mathews 1967; Laor & Draine 1993). On the other hand, for sufficiently large potentials, the

electrostatic stress exceeds the tensile strength of the grain material and the grain explodes. In this section, we estimate grain potentials and lifetimes for conditions likely to characterize BALQSO outflows.

10.1. Grain Charging

We adopt the unobscured quasar spectrum from Sazonov et al. (2004), given by

$$u_E = \alpha \begin{cases} 0.0798(E/\text{eV})^{-0.6} & , 1 \text{ eV} \leq E < 10 \text{ eV} \\ (E/\text{eV})^{-1.7} \exp(E/2 \text{ keV}) & , 10 \text{ eV} \leq E < 2 \text{ keV} \\ 2.94 \times 10^{-3} (E/\text{eV})^{-0.8} \exp(-E/200 \text{ keV}) & , E \geq 2 \text{ keV} \end{cases} . \quad (29)$$

The normalization constant $\alpha = 3.07 \text{ eV}^{-1} u(> 13.6 \text{ eV}) = 2.26 \times 10^{-10} \text{ erg eV}^{-1} n_\gamma(> 13.6 \text{ eV})$, where $u(> 13.6 \text{ eV}) [n_\gamma(> 13.6 \text{ eV})]$ is the total energy density [photon number density] beyond 13.6 eV. We consider gas temperatures $T = 10^4, 10^5, \text{ and } 10^6 \text{ K}$ and ionization parameters $U \equiv n_\gamma(> 13.6 \text{ eV})/n_{\text{H}} = 0.1, 1, 10, \text{ and } 10^2$.

Figures 6a and 7a display the grain potential ϕ for carbonaceous and silicate grains as a function of size. For comparison, Figures 6b and 7b display the potentials computed using the WD01 photoelectric yields; in this case, we only include photoelectric emission from the band structure, photodetachment, and collisional charging (including secondary emission induced by colliding gas-phase electrons). The use of our new, more realistic yields for photoelectric emission from the band structure substantially reduces the computed potential, despite the additional charging due to the emission of inner shell and Auger electrons (which account for at most $\approx 30\%$ of the charging) and the emission of photo-induced secondaries (which account for at most 2% of the charging). Secondary emission induced by gas-phase electrons contributes at most at the 5, 10, and 25% levels for $U = 10^2, 10, \text{ and } 1$, respectively. For $U = 0.1$ and $T = 10^6 \text{ K}$, this process dominates the grain charging. The “notches” at the far left in Figure 6a arise because we adopt higher yields for photoelectric emission from the band structure of carbonaceous grains with $a < 13 \text{ \AA}$ (eq. 15). To test how sensitive the results are to uncertainties in the photoelectric yield, we computed the potentials for the case that $U = 10$ and $T = 10^5 \text{ K}$ but with the adopted bulk yields multiplied by a factor of 2 or 0.5. The largest changes in the potential were by factors 1.3 and 0.75.

10.2. Grain Destruction

10.2.1. Coulomb Explosions

The electrostatic stress on a spherical grain is $S = (\phi/a)^2/4\pi$; if S exceeds the tensile strength S_{\max} , then the grain fragments (Draine & Salpeter 1979; Waxman & Draine 2000; Fruchter et al. 2001). Real grains are not perfectly spherical and the structure of grain material is poorly known; thus S_{\max} is highly uncertain. The maximum grain potential for which fragmentation will not occur is

$$\phi_{\max} = 1.06 \times 10^3 \text{ V} \left(\frac{S_{\max}}{10^{10} \text{ dyn cm}^{-2}} \right)^{1/2} \left(\frac{a}{0.1 \mu\text{m}} \right) . \quad (30)$$

If $S_{\max} \approx 10^{11} \text{ dyn cm}^{-2}$, as measured for ideal materials, then ion field emission, rather than Coulomb explosions, may limit the positive grain charge (Waxman & Draine 2000).

Figures 6a and 7a show the locus for Coulomb explosions for two possible values S_{\max} of the tensile strength. The results in Figures 6a and 7a show that if $S_{\max} \approx 10^{10} \text{ dyn cm}^{-2}$, then for ionization parameter $U \gtrsim 10$, Coulomb explosions result in a minimum grain radius of several $\times 10^{-3} \mu\text{m}$. However, electrostatic stresses reach $10^{11} \text{ dyn cm}^{-2}$ only for the smallest grains and very high values of U .

10.2.2. Thermal Sputtering

The cross section for a collision between an ion with charge $z_i e$ and energy E_i and a grain with radius a and potential ϕ is

$$\sigma = \pi a^2 \times \begin{cases} 1 - z_i e \phi / E_i & , E_i > z_i e \phi \\ 0 & , E_i \leq z_i e \phi \end{cases} . \quad (31)$$

Note that we have neglected the polarization of the grain by the ion. Integrating over a Maxwell speed distribution and summing over the various ions in the gas yields the sputtering rate for the case that $\phi \geq 0$:

$$\frac{1}{n_{\text{H}}} \frac{da}{dt} = \frac{2\pi\mu m_p}{\rho} (2\pi kT)^{-3/2} \sum_i \frac{n_i}{n_{\text{H}}} m_i^{-1/2} \int_{z_i e \phi}^{\infty} dE_i E_i \exp(-E_i/kT) \left(1 - \frac{z_i e \phi}{E_i} \right) Y_{s,i}(E_i - z_i e \phi) , \quad (32)$$

where ρ is the mass density of the grain material, μm_p is the average mass of the grain constituent atoms, m_i is the mass of ion i , n_i is the number density of ion i , and $Y_{s,i}$ is the sputtering yield for ion i (i.e., the probability that an atom from the grain is ejected following

a collision with a gas-phase ion). For the case that all of the ions are singly ionized,

$$\frac{1}{n_{\text{H}}} \frac{da}{dt} = \exp(-e\phi/kT) \frac{1}{n_{\text{H}}} \frac{da}{dt} \Big|_{\phi=0} . \quad (33)$$

For the Sazonov et al. (2004) spectrum (eq. 29),

$$n_{\gamma}(> 13.6 \text{ eV}) = 2.00 \times 10^7 \text{ cm}^{-3} \left(\frac{L}{10^{46} \text{ erg s}^{-1}} \right) \left(\frac{r}{\text{pc}} \right)^{-2} , \quad (34)$$

where L is the luminosity of the quasar between 1 eV and 10 keV and r is the distance to the central source. Combining equations (33) and (34) yields the following expression for the lifetime of a grain with radius a against thermal sputtering:

$$\tau_{\text{ts}} = 5.00 \text{ yr} \left(\frac{a}{0.1 \mu\text{m}} \right) \left(\frac{U}{10} \right) \left(\frac{L}{10^{46} \text{ erg s}^{-1}} \right)^{-1} \left(\frac{r}{\text{pc}} \right)^2 \left(\frac{n_{\text{H}}^{-1} da/dt(\phi=0)}{-10^{-4} \text{ cm}^3 \text{ \AA yr}^{-1}} \right)^{-1} \langle \exp(e\phi/kT) \rangle_a , \quad (35)$$

where

$$\langle \exp(e\phi/kT) \rangle_a \equiv \frac{1}{a} \int_{a_{\text{min}}}^a da' \exp[e\phi(a')/kT] . \quad (36)$$

We take $a_{\text{min}} = 5 \text{ \AA}$ and use the equilibrium charge for each grain size, rather than summing over the charge distribution. Tielens et al (1994) reexamined thermal sputtering as a function of gas temperature, obtaining rates very similar to those found by Draine & Salpeter (1979). We adopt the approximate expression from Tielens et al. (1994) for the thermal sputtering rate for neutral grains (their eq. 4.21 and Table 4); these were derived assuming that H, He, C, N, and O are all singly ionized and have solar abundances.

Figure 8 displays the ratio $\langle \exp(e\phi/kT) \rangle_a$ of τ_{ts} to the value it would take if the grains were uncharged. Figure 9 presents thermal sputtering lifetimes for grains with $a = 0.3 \mu\text{m}$ when $L = 10^{46} \text{ erg s}^{-1}$ and $r = 3 \text{ pc}$. The horizontal long-dashed line is the outflow timescale $\tau_{\text{flow}} = r/v \sim 100 \text{ yr}(r/3 \text{ pc})$ if the flow speed $v \sim 3 \times 10^4 \text{ km s}^{-1}$. The grains survive only for quite large values of the ionization parameter or low values of the gas temperature. Furthermore, when $U \gtrsim 10$, grains with $a \approx 0.3 \mu\text{m}$ experience supersonic drift relative to the gas, increasing the destruction rate. Thus, the lack of nuclear reddening in BALQSOs does not appear to require that the outflow originates in a dust-free region (e.g., within the sublimation radius). However, better observational constraints on the location and physical conditions in the outflow are needed before a firm conclusion can be reached.

11. Summary

In this paper, we have extended the WD01 photoelectric emission model to higher photon energies, enabling the treatment of dust exposed to hard radiation fields. We provide revised yields for photoelectric emission from the band structure when $h\nu > 20$ eV and treat the emission of Auger electrons and secondary electrons excited by primary and Auger electrons.

For HII regions, ionized by OB stars, the radiation field is soft enough that the WD01 model can be employed without modification; the new treatment yields a $\lesssim 10\%$ difference in the gas heating rate.

For planetary nebulae, the gas heating rates found with the extended model are lower, by a factor 2 or less, than those estimated with the WD01 model, since the revised yields for photoelectric emission from the band structure are lower. Inner shell, Auger, and secondary emission are not important. For quasar outflows, the new treatment yields significantly lower grain potentials. In this case, combined inner shell and Auger emission contribute at as high as the 30% level. This is less than the uncertainty associated with photoelectric emission from only the band structure. Secondary emission is unimportant. It appears that thermal sputtering can destroy dust in BALQSO outflows in less than a dynamical time, for a wide range of plausible physical conditions in the outflow. However, better constraints on the outflow conditions are needed to definitively settle the issue of dust survivability.

In environments with harder radiation fields (e.g. supernova remnants and the central regions of galaxy clusters), inner shell, Auger, and secondary emission may be more important relative to photoelectric emission from the band structure. However, in these cases the gas is so hot that secondary emission induced by gas-phase electrons and ions incident on the grain is expected to dominate over photoelectric emission in grain charging (Draine & Salpeter 1979).

Support for this work, part of the Spitzer Space Telescope Theoretical Research Program, was provided by NASA through a contract issued by the Jet Propulsion Laboratory, California Institute of Technology under a contract with NASA. BTM was supported in part by NSF grant AST-0406883. We are grateful to Norm Murray, Gary Ferland, and Peter van Hoof for helpful discussions.

REFERENCES

Bakes, E. L. O., & Tielens, A. G. G. M. 1994, *ApJ*, 427, 822

- de Jong, T. 1977, *A&A*, 55, 137
- Dopita, M. A. & Sutherland, R. S. 2000, *ApJ*, 539, 742
- Draine, B. T. 1978, *ApJS*, 36, 595
- Draine, B. T. 2003, *ApJ*, 598, 1026
- Draine, B. T. & Salpeter, E. E. 1979, *ApJ*, 231, 77
- Draine, B. T. & Sutin, B. 1987, *ApJ*, 320, 803
- Dwek, E. & Smith, R. K. 1996, *ApJ*, 459, 686
- Ferland, G. J., Martin, P. G., van Hoof, P. A. M., & Weingartner, J. C. 2002, in Workshop on X-ray Spectroscopy of AGN with Chandra and XMM-Newton, MPE Report 279, 103
- Fruchter, A., Krolik, J. H., Rhoads, J. E. 2001, *ApJ*, 563, 597
- Gallagher, S. C., Brandt, W. N., Chartas, G., & Garmire, G. P. 2002, *ApJ*, 567, 37
- Horányi, M. 1996, *ARA&A*, 34, 383
- Laor, A. & Draine, B. T. 1993, *ApJ*, 402, 441
- Li, A. & Draine, B. T. 2001, *ApJ*, 554, 778
- Martin, C., Arakawa, E. T., Callcott, T. A., & Warmack, R. J. 1987, *J. Electr. Spectrosc. Rel. Phenom.*, 42, 171
- McFeely, F. R., Cartier, E., Yarmoff, J. A., & Joyce, S. A. 1990, *Phys. Rev. B*, 42, 5191
- Mathews, W. G. 1967, *ApJ*, 147, 965
- Reichard, T. A. et al. 2003, *AJ*, 126, 2594
- Sazonov, S. Y., Ostriker, J. P., & Sunyaev, R. A. 2004, *MNRAS*, 347, 144
- Spitzer, L., Jr. 1948, *ApJ*, 107, 6
- Tielens, A. G. G. M., & Hollenbach, D. J. 1985, *ApJ*, 291, 722
- Tielens, A. G. G. M., McKee, C. F., Seab, C. G., & Hollenbach, D. J. 1994, *ApJ*, 431, 321

- van Hoof, P. A. M., Weingartner, J. C., Martin, P. G., Volk, K., & Ferland, G. J. 2004, MNRAS, 350, 1330
- Verner, D. A., Ferland, G. J., Korista, K. T., & Yakovlev, D. G. 1996, ApJ, 465, 487
- Verner, D. A. & Yakovlev, D. G. 1995, A&AS, 109, 125
- Watson, W. D. 1972, ApJ, 176, 103
- Watson, W. D. 1973, J. Opt. Soc. Am., 63, 164
- Waxman, E. & Draine, B. T. 2000, ApJ, 537, 796
- Weingartner, J. C. & Draine, B. T. 2001a, ApJ, 548, 296
- Weingartner, J. C. & Draine, B. T. 2001b, ApJS, 134, 263 (WD01)

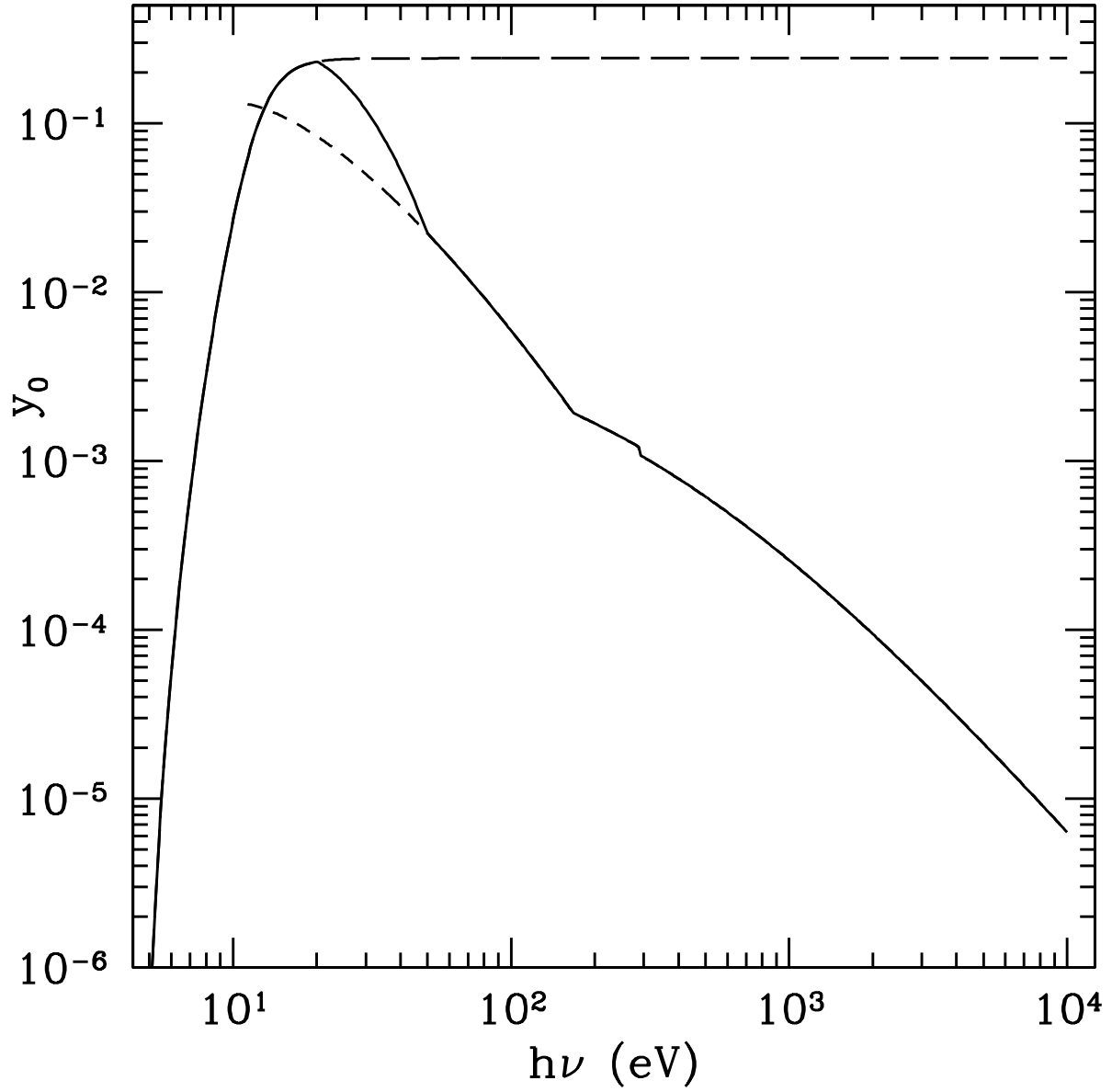


Fig. 1.— Bulk yield for carbonaceous dust. Long-dashed curve: WD01 yield; short-dashed: yield computed with eq. (9); solid: our adopted yield

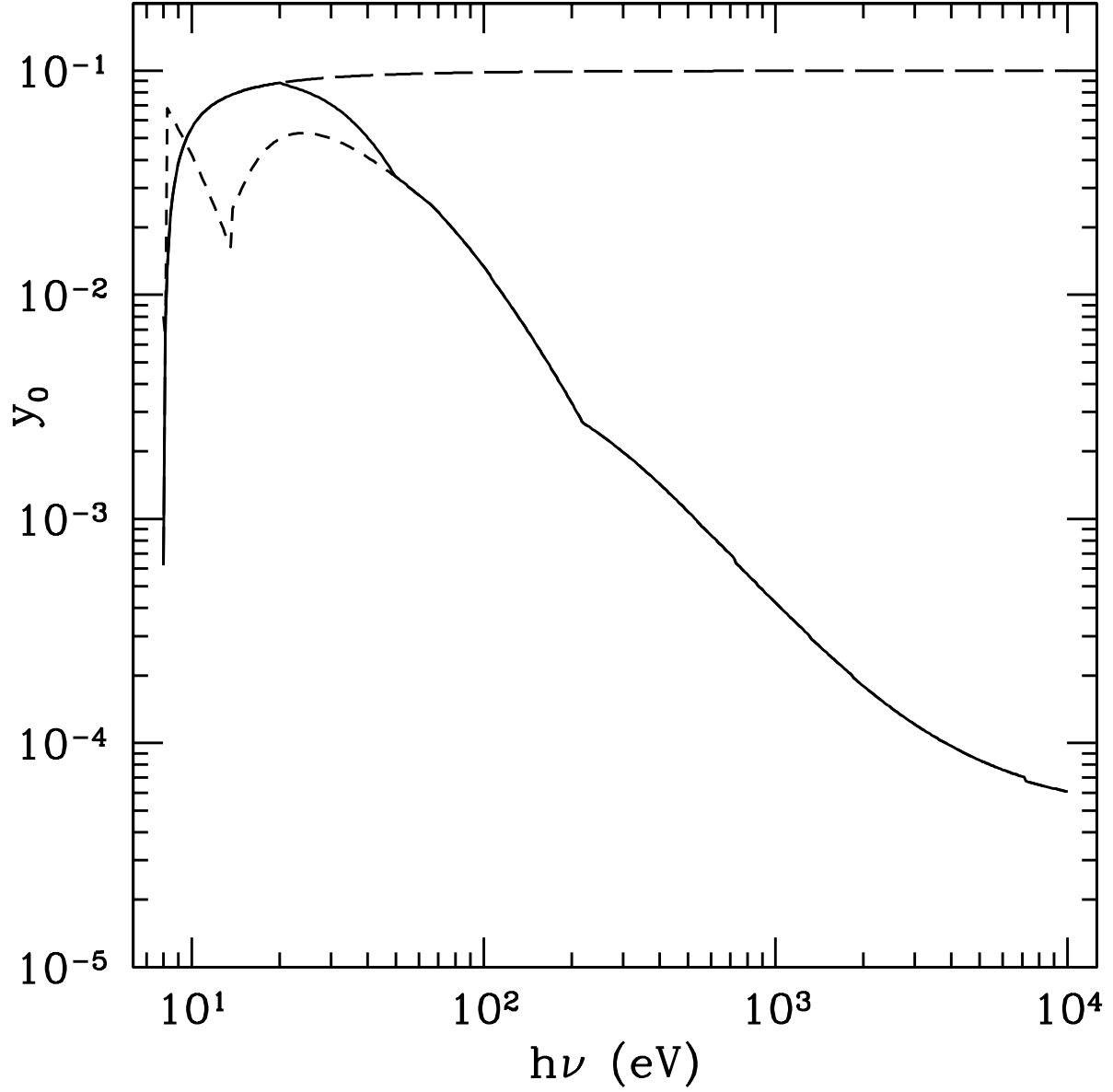


Fig. 2.— Bulk yield for silicate dust. Long-dashed curve: WD01 yield; short-dashed: yield computed with eq. (9); solid: our adopted yield

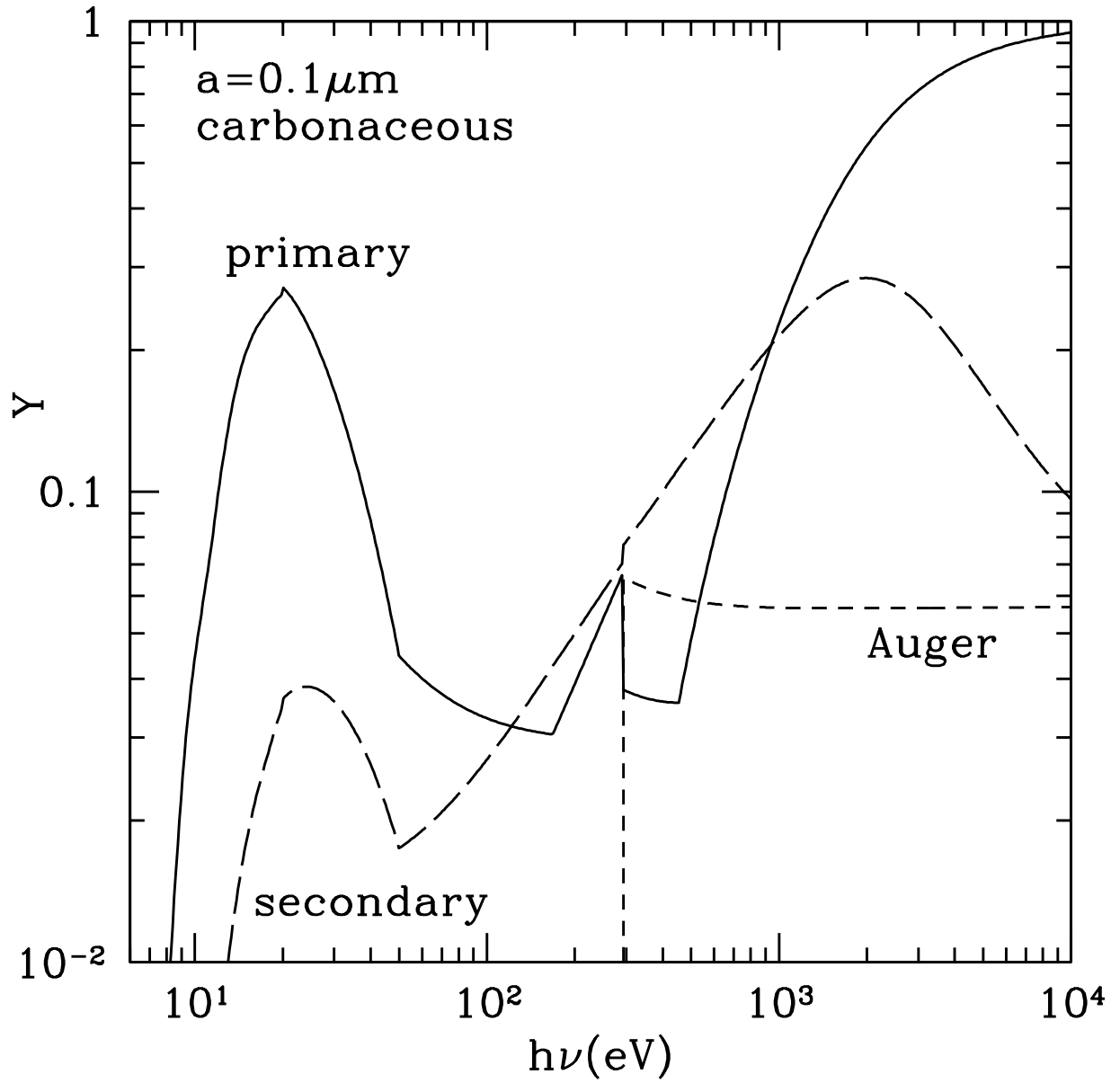


Fig. 3.— The yields of primary, Auger, and secondary electrons for uncharged carbonaceous grains with $a = 0.1 \mu\text{m}$.

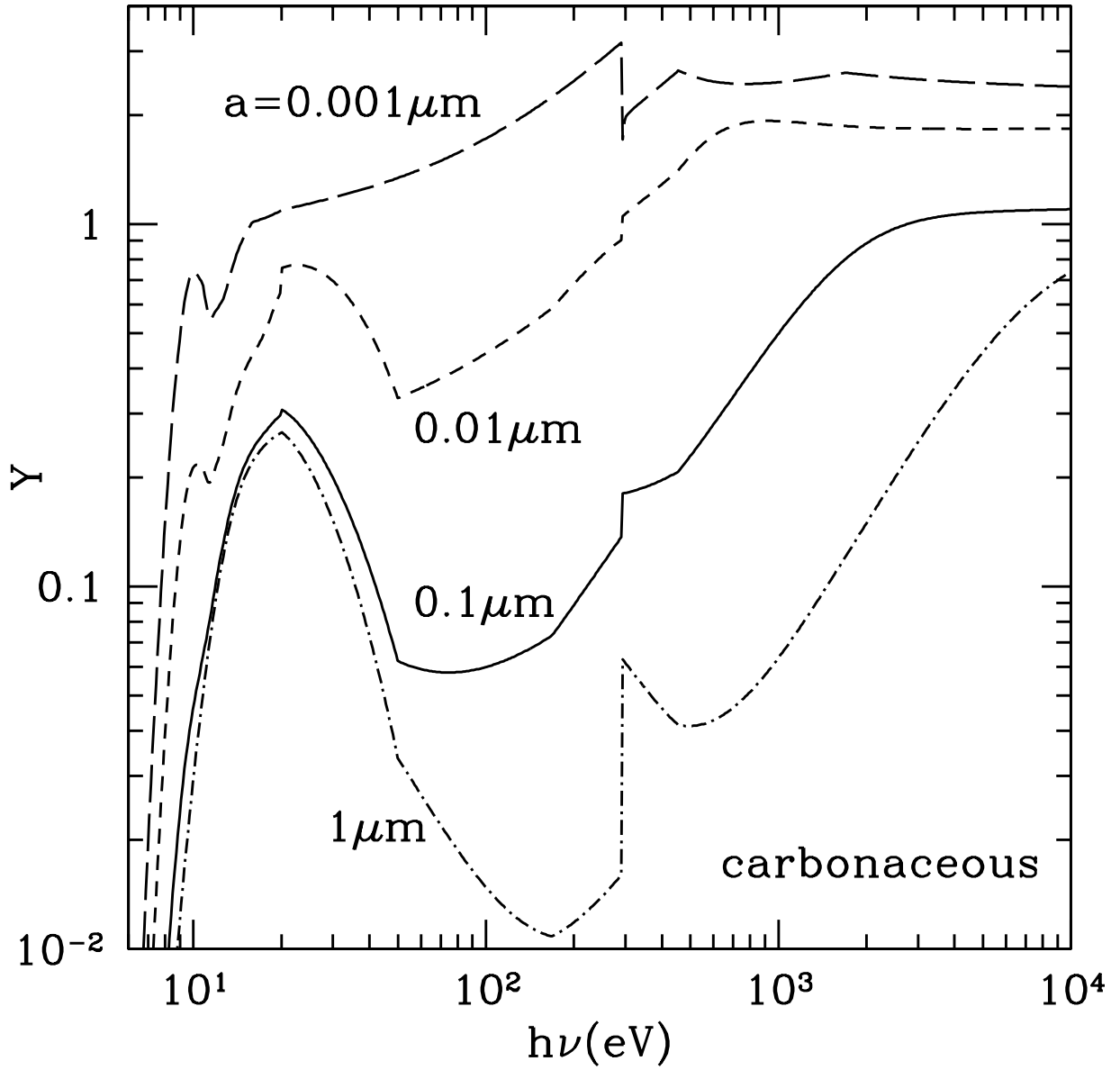


Fig. 4.— The total yield (primary plus Auger plus secondary) for uncharged carbonaceous grains of four different sizes, as labelled.

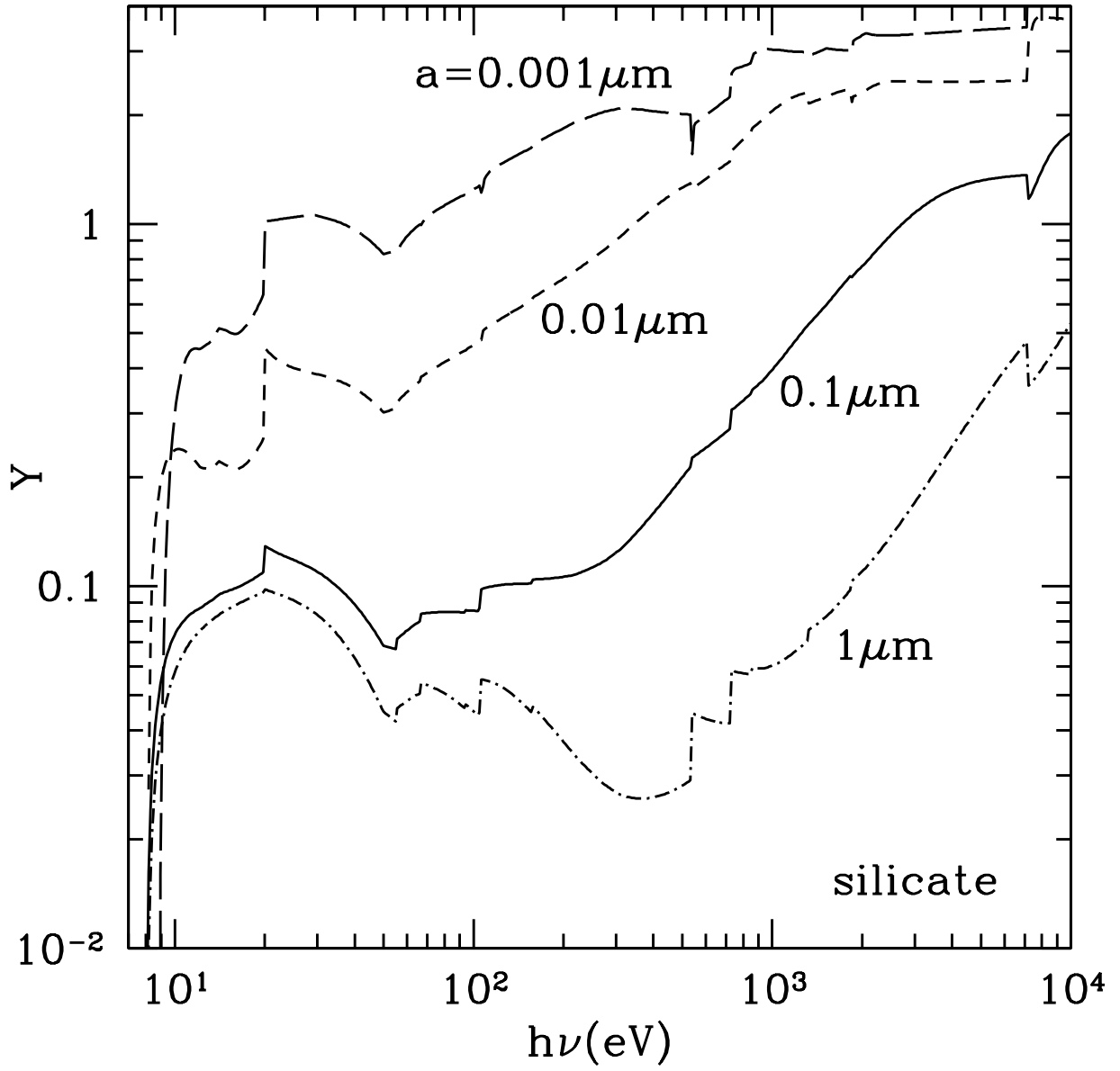


Fig. 5.— Same as Fig. 4, except for uncharged silicate grains.

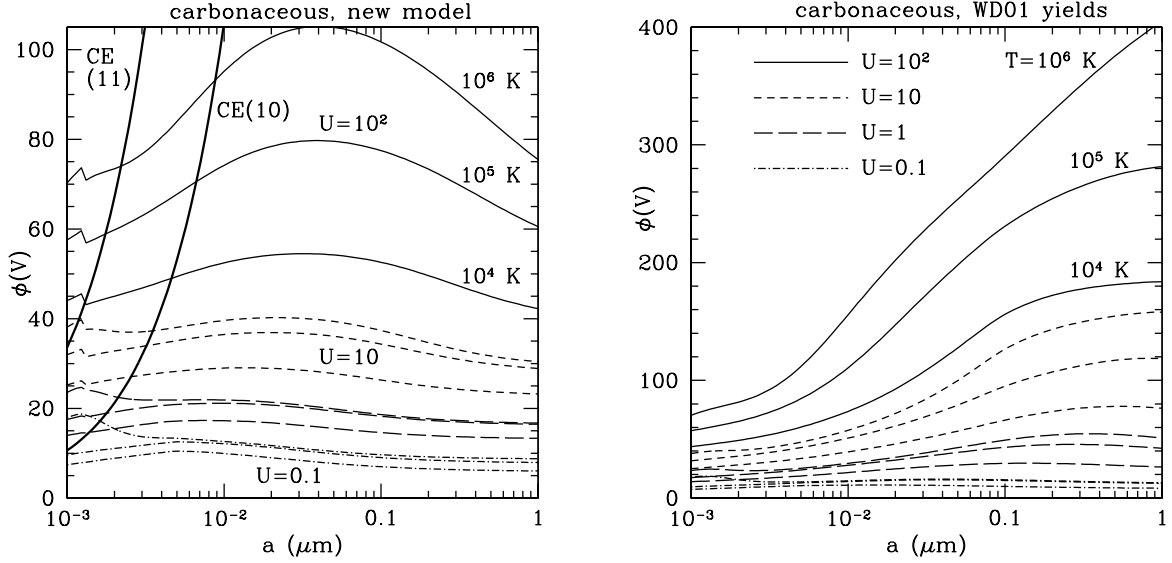


Fig. 6.— (a) Carbonaceous grain potential ϕ versus radius a for grains exposed to an unobscured quasar spectrum (eq. 29) with ionization parameter $U = 0.1, 1, 10,$ and 10^2 , and for gas temperatures $T = 10^4, 10^5,$ and 10^6 K, as indicated. For a given value of U , the potential is larger for higher T . Coulomb explosions occur to the left of the heavy curve labelled “CE(10)” if the tensile strength $S_{\text{max}} \approx 10^{10} \text{ dyn cm}^{-2}$ and to the left of the curve labelled “CE(11)” if $S_{\text{max}} \approx 10^{11} \text{ dyn cm}^{-2}$. (b) Computed grain potentials using the photoelectric yields from WD01, for comparison.

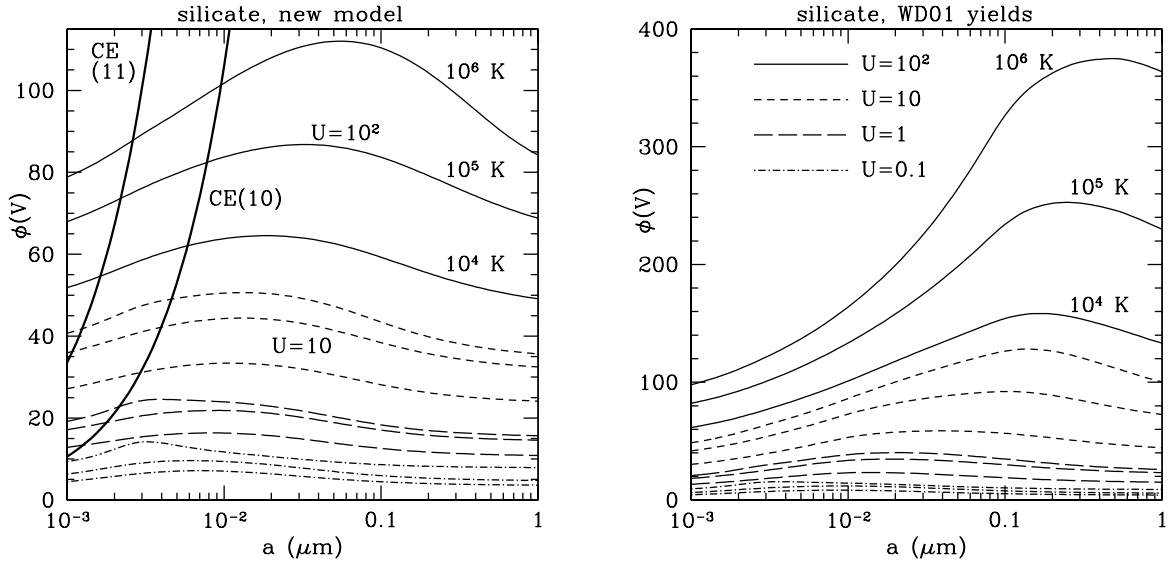


Fig. 7.— Same as Fig. 6, except for silicate grains.

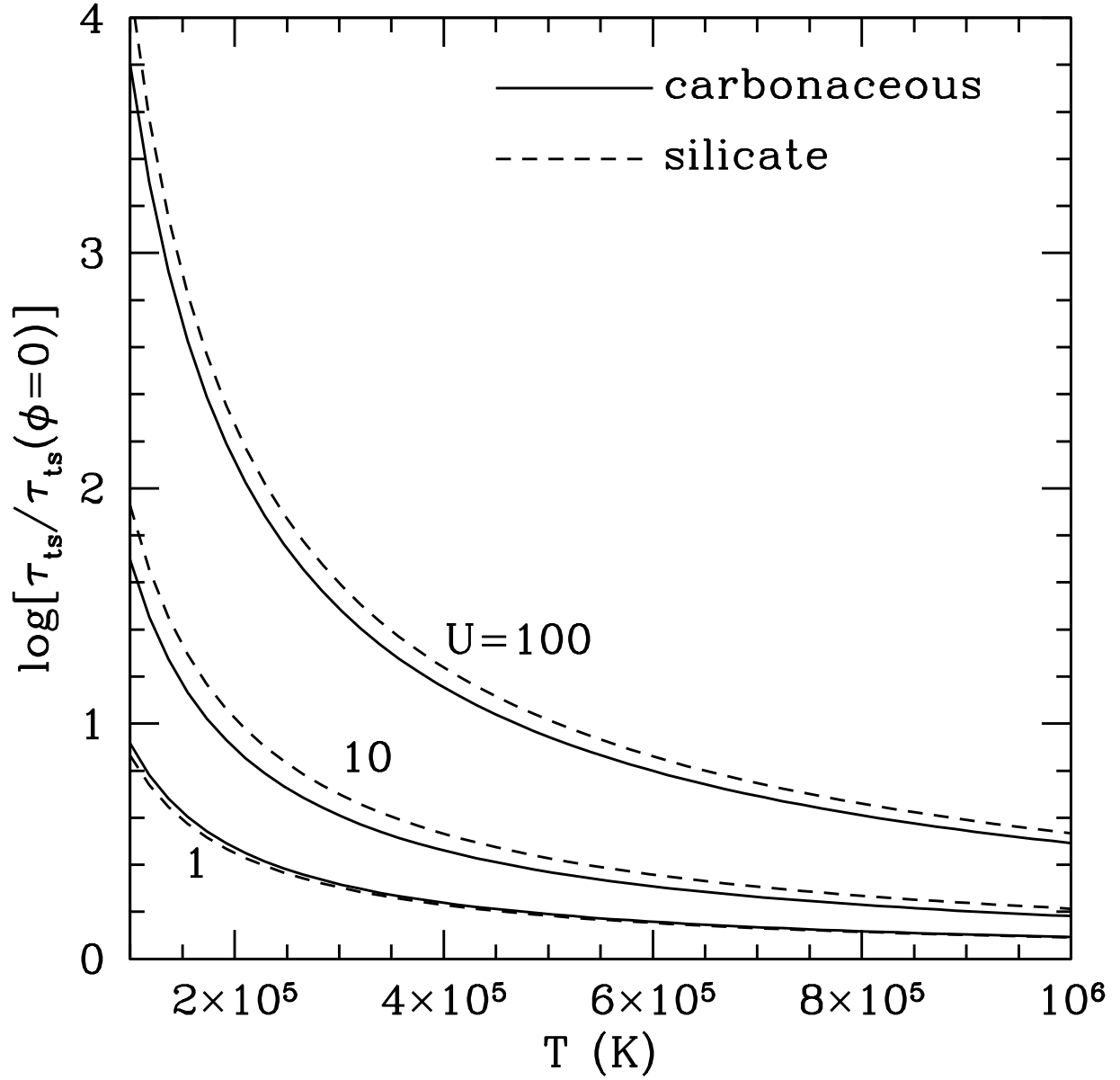


Fig. 8.— Ratio of the thermal sputtering timescale to its value for uncharged grains, versus gas temperature.

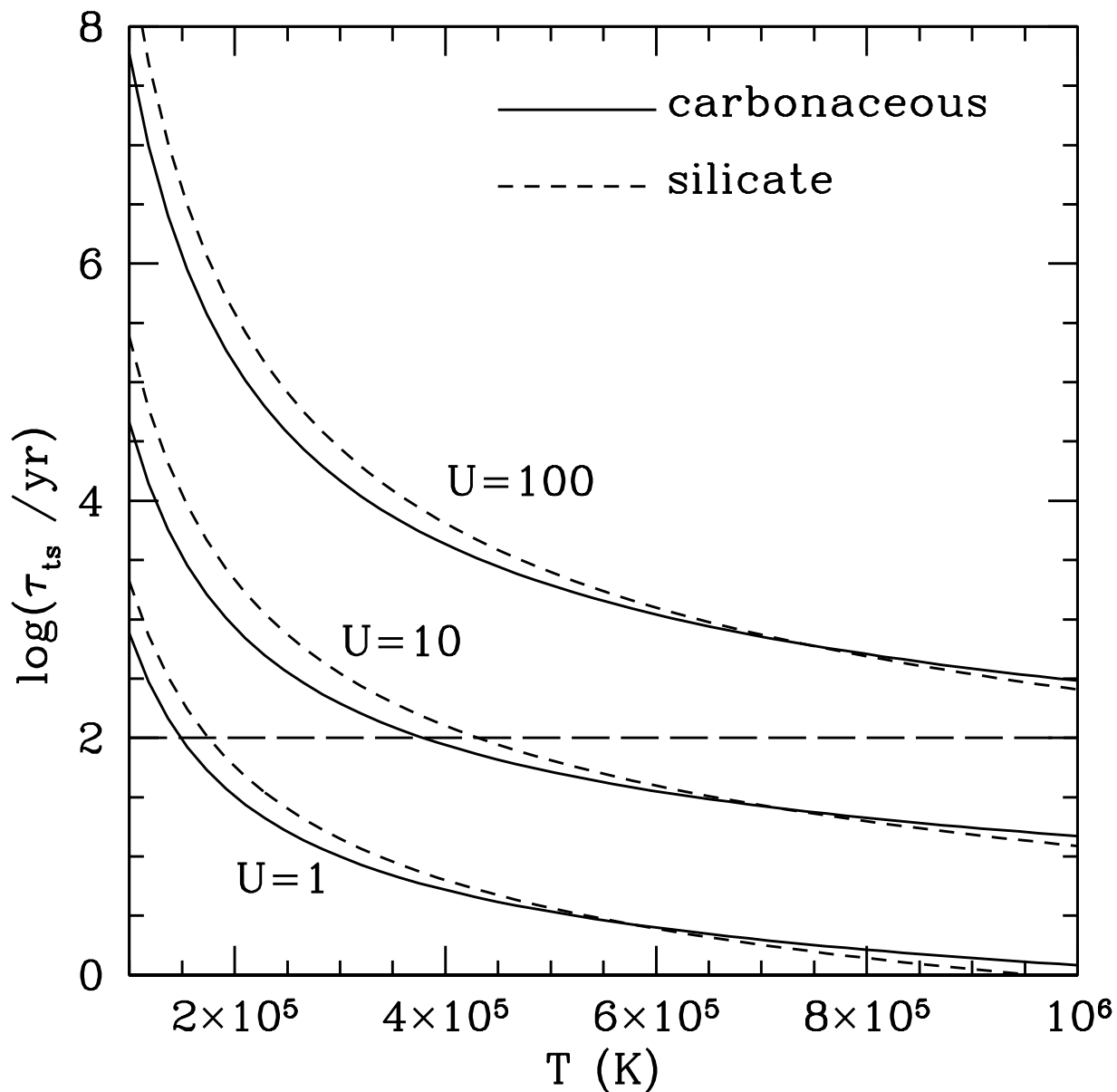


Fig. 9.— Thermal sputtering lifetime τ_{ts} for grains with $a = 0.3\mu\text{m}$ when $L = 10^{46} \text{ erg s}^{-1}$ and $r = 3 \text{ pc}$, versus gas temperature. The horizontal long-dashed line is the outflow timescale τ_{flow} , assuming that the outflow speed $v \sim 3 \times 10^4 \text{ km s}^{-1}$.

Table 1. Ionization Energies^a

Element	1s	2s	2p	3s	3p	3d	4s
C	291	19.39	11.26
O	538	28.48	13.62
Mg	1311	94.0	54.9	7.646
Si	1846	156	106	15.17	8.152
Fe	7124	857	724	104	66	14.7	7.902

^ain eV

Table 2. Photoelectric Heating and Recombination Cooling Rates for a Model Planetary Nebula

composition	R_V	$10^5 b_C$	case	$\Gamma_{pe}/(Gn_H)^a$	$\Lambda/(Gn_H)^a$
carbon	3.1	0.	A	16.2	1.97
carbon	3.1	6.	A	45.9	5.56
carbon	4.0	0.	A	12.8	1.55
carbon	4.0	4.	A	31.6	3.82
carbon	5.5	0.	A	9.75	1.19
carbon	5.5	3.	A	23.4	2.84
carbon	4.0	0.	B	16.7	2.05
carbon	4.0	4.	B	32.0	3.89
carbon	5.5	0.	B	13.3	1.64
carbon	5.5	3.	B	22.6	2.75
silicate	3.1	0.	A	15.6	1.29
silicate	3.1	6.	A	22.5	1.89
silicate	4.0	0.	A	9.84	0.818
silicate	4.0	4.	A	9.31	0.775
silicate	5.5	0.	A	3.83	0.314
silicate	5.5	3.	A	3.61	0.297
silicate	4.0	0.	B	10.1	0.840
silicate	4.0	4.	B	9.73	0.810
silicate	5.5	0.	B	3.87	0.316
silicate	5.5	3.	B	3.84	0.314

^a $10^{-25} \text{ erg s}^{-1}$